Precise motor rhythmicity relies on motor network responsivity

Kazumasa Uehara[1,2,3], Hiroki Togo[1,4], Takashi Hanakawa[1,4*]

1. Department of Advanced Neuroimaging, Integrative Brain Imaging Center, National Center of Neurology and Psychiatry, Kodaira, Tokyo, Japan
2. Division of Neural Dynamics, Department of System Neuroscience, National Institute for Physiological Sciences, Okazaki, Aichi, Japan
3. Department of Physiological Sciences, School of Life Sciences, SOKENDAI (The Graduate University of Advanced Studies), Okazaki, Aichi, Japan
4. Department of Integrated Neuroanatomy and Neuroimaging, Kyoto University Graduate School of Medicine, Kyoto, Japan

Abstract

Rhythmic movements are the building blocks of human behavior. However, given that rhythmic movements are achieved through complex interactions between neural modules, it remains difficult to clarify how the central nervous system controls motor rhythmicity. Here, using a novel tempo- precision trade-off paradigm, we first modeled interindividual behavioral differences in tempo-dependent rhythmicity for various external tempi. We identified two behavioral extremes: conventional and paradoxical tempo-precision trade-off types. We then explored the neural substrates of these behavioral differences using task and resting-state functional magnetic resonance imaging. We found that the responsibility of interhemispheric motor network connectivity to tempi was a key to the behavioral repertoire. In the paradoxical trade-off type, interhemispheric connectivity was low at baseline, but increased in response to increasing tempo; in the conventional trade-off type, strong baseline connectivity was coupled with low responsivity. These findings suggest that tunable interhemispheric connectivity underlies tempo-dependent rhythmicity control.

Key words: Motor rhythmicity, Individual variability, Primary motor cortex, Task-evoked functional connectivity, Resting-state connectivity

Introduction

Rhythmic movement is a building block of human motor behavior, and provides the foundation for skilled movements, such as those required for typing, playing instruments, and sports activities. Rhythmic movements are not mere repetitions of discrete movements (Schaal et al. 2004; Ikegami et al. 2010) but are uniquely hierarchical. The periodic neural activity necessary for rhythmic movement can be automatically generated by the central pattern generator (CPG) in the brainstem and spinal cord (Eve Marder and Dirk Bucher 2001; Grillner 2006). Supraspinal inputs to the CPG from cortical or subcortical motor areas are critical for the initiation, maintenance, and termination of rhythmic movements (Degallier and Ijspeert 2010). Furthermore, cortical motor areas regulate patterns of rhythmic movement, especially for precise regulation of motor timing relative to external rhythms (Schaal et al. 2004; Aso et al. 2010; Uehara et al. 2011; Pflug et al. 2019). The fronto-parietal associative regions, especially the dorsolateral prefrontal cortex (DLPFC) and the supramarginal gyrus (SMG), may also be required for rhythmic actions (Wiener et al. 2012; Hayashi et al. 2015). However, the neural machinery underlying rhythmic movement is not yet fully understood.

Rhythmicity is modulated by tempo, which is the speed at which rhythmic actions are performed and is typically referred to in the context of playing music. Changes in tempo during rhythmic movement strongly modulate brain activity of motor-related networks (Sadato et al. 1996, 1997; Toma et al. 2002; Witt et al. 2008; Hanakawa et al. 2017). To adapt to a fast tempo, the strategy is to sacrifice either accuracy or speed (Fitts 1954; Reis et al. 2009; Dayan and Cohen 2011; Shmuelof et al. 2012), indicating that individuals must adjust the relationship between accuracy and speed for different tempi. Interestingly, accuracy may also be sacrificed to keep a slow tempo (Reep and Rebercca 2007). Thus, individuals may show substantially different patterns of adjustment to cope with different tempi during rhythmic movements (Grahn and Schuit 2012). However, it remains open to debate as to how individual variability in adjusting rhythmic movements at different movement tempi should be quantified. In this report, we describe a novel function, namely the tempo-rhythmicity function (TRF). This function can represent behavioral traits of tempo-dependent rhythmicity, which we identified using a tempo-precision trade-off paradigm.

Moreover, it remains unclear how the multi-level central nervous system can adjust tempo-dependent rhythmicity, particularly 1) which brain regions or networks were correlated with individual differences in TRF, and 2) whether the network properties in different task conditions (tapping vs. resting state) were coupled with consonant or dissonant aspects of the TRF. Using functional magnetic resonance imaging (fMRI), we analyzed task-evoked brain activity to define brain regions involved in tempo-dependent rhythmicity. We then investigated whether task-evoked and/or resting-state connectivity underlie individual differences in the control of motor rhythmicity.

The contralateral primary motor cortex (M1) is crucial for the control of rhythmic movement and movement timing (Toma et al. 2002; Schaal et al. 2004; Witt et al. 2008). Notably, M1 ipsilateral to the movement side also encodes neural information related to motor actions (Fujiwara et al. 2017; Berlot et al. 2019; Yokoi and Diedrichsen 2019; Iwama et al. 2020). Specifically, the ipsilateral M1 may encode information on movement timing when performing unilateral repetitive finger movements (Chen et al. 1997), and its excitability is modulated by tapping tempo (Uehara et al. 2011, 2013). Based on these findings, we hypothesized that interhemispheric M1 connections might play a pivotal role in the control of tempo-dependent rhythmicity during unilateral movements. However, another line of evidence indicates that motor rhythm guided by auditory stimuli is represented in the fronto-parietal network including SMG (Konoike et al. 2015). From the viewpoint of inter-individual variations, SMG activity represents inter-individual variation of pitch and rhythm memory (Schaal et al. 2017). DLPFC is also essential for timing control (Jones et al. 2004; Koch et al. 2007; Yin et al. 2019). Based on these empirical findings, we developed an alternative hypothesis on the involvement of the fronto-parietal network in the control of tempo-dependent rhythmicity. Furthermore, we posed an additional hypothesis on the individual differences in baseline functional connectivity underlying those of motor rhythmicity. The spontaneous fluctuations of network activity at a resting state have been thought to contain patterns that are also seen in task-evoked or sensory-induced brain activity

(Kenet et al. 2003; Luczak et al. 2009, 2013; Berkes et al. 2011). Given this, resting-state connectivity should have a close relationship with movement at slow tempi because the rhythmicity-relevant network would experience a longer idling state (similar to the resting state) during slow tempi than during fast tempi.

Methods and Materials

Participants

Twenty-nine participants (12 females) participated in the main experiment. However, six out of 29 participants were excluded from the final analyses due to extensive head motion during MRI scans (the *a priori* criterion for acceptable head displacement was less than 3 mm in any direction) or the failure of the performance of finger taps for several seconds during the tapping blocks. Thus, data from a final total of 23 participants were reported. To confirm the novel findings of the tempo-precision trade-off, data from additional 12 participants (6 females) who participated in a different experiment were analyzed. Thus, data from a total of 41 participants with a mean age of 26.1 ± 4.2 years (mean ± standard deviation (SD), range: 20-36 years) were subjected to the TRF analysis. Handedness was assessed by the Edinburgh Handedness Inventory (Oldfield 1971). All participants were naïve to the purpose of this study. None of the participants had any history of neurological or psychiatric disorders and they had not received any intensive musical training as musicians. The experimental protocol was approved by the ethics committee of the National Center of Neurology and Psychiatry, Kodaira, Japan. All participants gave written informed consent.

Experimental tasks

Resting-state and task- fMRI

All participants underwent resting-state fMRI before the task-fMRI. They first underwent resting-state fMRI, which required a 10-min maintenance of the resting state without thinking of anything particular with their eyes open. The fixation cross was projected onto the center of the screen in the scanner.

In the following task-fMRI scans, participants were given the familiarization exercise before starting the first task-fMRI scan. The tapping task was arranged in blocks, each lasting for 20 s, and was interleaved with 20-s rest blocks. During the task blocks, participants performed a repetitive finger tapping at five different tempi (0.25, 1, 2, 3, and 4 Hz) with their right index finger. They were asked to tap as precisely as possible while synchronizing with the auditory cues (100-ms duration each) presented at the five different tempi. The fixation cross was always presented, along with the "*Go*" cue during task blocks and the "*Rest*" cue during rest blocks. During each rest block, we provided the same auditory cues that would be given in the consecutive task block. The order of the tempi was semi-randomized between blocks, and the same tapping tempo was not presented in consecutive blocks. Presentation software (Neurobehavioral systems, USA) was used to control the task paradigm, synchronize events with the MRI scanning, and record finger tapping timing. All participants completed three task-fMRI runs. Each run consisted of two blocks of each tapping tempo (i.e., 10 task blocks per run). To acquire behavioral information during the tapping tasks, an MRI-compatible response button device was

used (HHSC-1 × 4-CL, Current designs Inc., USA).

Data acquisition

MRI data acquisition

Images were acquired using a 3-Tesla Magnetom Verio Dot MRI scanner (Siemens Medical Systems, Germany). The task- and resting-state fMRI data were acquired via an echo planar imaging (EPI) sequence sensitive to blood-oxygen-level-dependent (BOLD) signals as follows: repetition time (TR) = 2500 ms; echo time (TE) = 30 ms; flip angle = 80°; field of view = 212×212 mm^2; 40 axial slices covering the whole brain; slice thickness = 3.2 mm with a 0.8 mm gap, yielding 3.3×3.3×4.0 mm^3 voxel size. Two field-map images were acquired in the same space as EPIs using the following parameters: TR = 488 ms; TE = 4.92/7.38 ms. For anatomical registration, T1-weighted three-dimensional structural images were also acquired using the magnetization-prepared rapid gradient-echo sequence (MPRAGE) with the following parameters: TR = 1900 ms; TE = 2.52 ms; inversion time (TI) = 900 ms; flip angle = 9°; field of view = 250×250 mm^2; acquisition matrix = 256×256; slice thickness = 1.0 mm without a gap; axial slice number = 192; voxel dimension = 1.00×0.97×0.97 mm^3.

fMRI data preprocessing

Image preprocessing for the task-fMRI data was carried out using FMRIB's Software Library (FSL6.00, http://www.fmrib.ox.ac.uk/fsl) and SPM12 (http://www.fil.ion.ucl.ac.uk/spm/) implemented in Matlab. The first four volumes from each experimental run were discarded to ensure stable magnetization. Field-map correction was applied to reduce distortions from magnetic field inhomogeneity using FSL's FUGUE. Distortion-corrected EPI images were fed into an independent component analysis (ICA) with FSL's Multivariate Exploratory Linear Optimized Decomposition into Independent Components (MELODIC) (Beckmann et al. 2005) to decompose single participants' 4-dimensional (4D) fMRI data sets into spatial and temporal components within each run. Subsequently, we applied automatic component classification with FMRIB's ICA-based X-noiseifier (FIX) to remove noise components automatically from the 4D fMRI data (Griffanti et al. 2014; Salimi-Khorshidi et al. 2014). To train the FIX's noise classifier, we used 25 runs during the finger tapping task from 29 participants randomly selected from this study (each participant was scanned three times; therefore, 87 runs were available). Noise ICA components for the FIX-training were identified using visual inspection, based on previous literature (Kelly et al. 2010). The FIX-cleaned fMRI data were then fed into SPM12 for further preprocessing, including realignment, slice timing correction, coregistration with structural images, normalization to the Montreal Neurological Institute (MNI) functional template, and smoothing using an isotropic Gaussian kernel of 8-mm full-width at half-maximum (FWHM).

For the resting-state fMRI data, field-map correction with FUGUE and ICA-based FIX were also applied. In this case, FIX was trained using resting-state fMRI data from 47 participants, 10 of whom were randomly selected from the present study and 37 of whom were taken from a different resting-state fMRI study acquired with the same scanner (Togo et al. 2017). The components identified as noise

were selected using visual inspection (Kelly et al. 2010). Preprocessing was conducted with the CONN functional connectivity toolbox (version 18.b.; https://www.nitrc.org/projects/conn) implemented in SPM12 (Whitfield-Gabrieli and Nieto-Castanon 2012). In particular, realignment, slice time correction, coregistration with structural images, normalization to the MNI functional template, and smoothing with an isotropic Gaussian kernel of 8-mm FWHM were performed. After preprocessing, the data were band-pass filtered at 0.01–0.09 Hz and motion scrubbed and motion regressed to reduce the influence of noise (Power et al. 2012). Finally, the remaining noise, including white matter, cerebrospinal fluid, and physiological noise, was taken as confounds using a CompCor algorithm based on principal component analysis (Behzadi et al. 2007; Whitfield-Gabrieli and Nieto-Castanon 2012).

Data analysis

Motor behavior

Motor performance was analyzed using a custom-written code implemented in Matlab (Mathworks, USA). As an index of motor rhythmicity, a coefficient of variation (CV) of inter-tap intervals (ITIs) was computed for each of the four tempi (1, 2, 3, and 4 Hz) in each participant, using the following formula: CV (%) = (ITI_{SD}/ITI_{Mean}) ×100. We used CV because we observed that CV of inter-tap (or keystroke) intervals reflected a motor skill and its degradation due to a disease process in our series of studies (Furuya et al. 2018; Kita et al. 2018, 2021). Note that we computed the CVs of each movement for the first 20 consecutive finger taps in each block. In the 1 Hz condition, some participants had less than the necessary number of finger taps (20 finger taps), because the last finger tap went out of the time range for the task block. In this case, we calculated the CV using the maximum number of finger taps. The 0.25 Hz condition was not used for this computation because of the small number of taps in each block. The CV values were first averaged in each tapping tempo at the individual level. Subsequently, the averaged CV values for each participant were then logarithmically transformed in order to meet the assumption of normal distribution before a linear fitting was performed. To quantify the relationships of the CV values to tapping tempi, the log-transformed CV values were fitted against tempo using a linear regression model within each participant, which yielded the TRF. This mathematical process was inspired by previous evidence for the speed-accuracy tradeoff behavior in which a linear relationship existed between movement accuracy and speed (Fitts 1954; Reis et al. 2009; Dayan and Cohen 2011; Shmuelof et al. 2012). This linear relation represents how much a participant sacrifices either accuracy or speed for faster movement.

Detailed model selection procedures are as follows: Before fitting the linear regression model, we calculated root mean squared error (RMSE) for each participant and then averaged this across participants to assess which of the linear or quadratic (non-linear) model was more suitable for modeling the effects of tempo onto CVs. This was because it was not clear if CV as a function of tempo should monotonically change, or it should show a vertex corresponding to the optimal tempo. We treated both intercepts and slopes obtained from the TRF as the main behavioral features in this study. The *slope* indicates how rhythmicity was maintained across different tempi. Positive and negative

slopes are indicative of worse and better rhythmicity, respectively, with faster tempi. The *intercept* extrapolated the linear relationship between tempo and rhythmicity to very slow tempi. Thus, this was considered to serve as a proxy measure for timing control of discrete movement (i.e., discrete timing). A large *intercept* indicates a less precision rhythmicity in discrete movement. The reason why we used the *intercept* as the index of discrete timing was that it could serve as a quantitative marker of rhythmicity at less than 1Hz more adequately than the measured values of CV at 0.25 Hz. As mentioned, the 0.25 Hz condition had a small number of taps in each block due to the methodological limitation of block-design fMRI, making the CV at 0.25 Hz less reliable. The *intercept* of TRF allows for a comprehensive assessment of the interplay between rhythmicity and discrete timing control and its neural substrates from the same dataset.

To test a relationship between the *slope* and *intercept* of the TRF, we computed Pearson's skipped correlations using the Robust Correlation Toolbox (Pernet et al. 2013) implemented in Matlab. To minimize the effect of possible outliers on the correlation analyses, we adopted a bootstrap approach. This method deals with bivariate outliers and computes statistical significance using a bootstrapped CI with 1,000 permutations that has an appropriate false-positive control. Correlations were considered significant if the 95% CI did not include zero.

In addition, temporal synchronization between each cue sound and each finger tap was calculated during the tapping task in each tempo. To quantify whether each participant made proactively or reactively each finger tap, the degree of temporal synchronization at each frequency was expressed as tapping cycle. A value of zero indicates their perfect synchronization. Less and more than zero indicates proactive and reactive tapping, respectively. Synchronization was analyzed using a two-way repeated measure and mixed design analysis of variance (ANOVA) with the "group" as the between-subject factor and "tapping tempo" as the within-subject factor, adjusted by Greenhouse-Geisser correction as the assumption of sphericity was violated. Post-hoc explorations using Bonferroni correction for multiple comparisons were performed if a significant effect was detected from ANOVA. Unless otherwise noted, statistical effects were tested at a significance level of $p < 0.05$ through the experiment and Pearson's skipped correlations with a bootstrap approach was used when a single correlation analysis was performed.

To test the replicability of the tempo-precision tradeoff behavior, we analyzed data from the 12 additional participants who participated in another experiment. This experiment was conducted in almost the same setting, but the tempo varied only between 1, 2 and 3 Hz. The CV values from 1 to 3 Hz were fitted using a linear regression model within each participant. Subsequently, we confirmed a correlation between the *slope* and *intercept* of the TRF, using Pearson's skipped correlation.

Statistical analysis for task- and resting-state fMRI scans

Tempo-modulated brain activity

The following statistical analyses were carried out using SPM12. We first computed a single-subject fixed-effects model for each participant. The signal time-course of each partic-

ipant was modeled with a boxcar function convolved with the canonical hemodynamic response function (HRF). Low-frequency noise was removed using a high-pass filter with a cut-off of 128 s, and serial correlations were adjusted using an auto-regression model. We conducted two GLM analyses. In the first analysis, we used a parametric design to identify brain activity that was correlated with the tapping tempo. A parametric regressor (modeling five tapping tempi: 0.25, 1, 2, 3, and 4 Hz) was created along with a repetitive state model for the tapping blocks. Note that even though the 0.25 Hz condition was not used to calculate the behavioral parameters (i.e., TRF), the 0.25 Hz condition was incorporated in this parametric regressor because we sought for the relationship between changes in brain activity or functional connectivity from the slow to fast tempi and the discrete timing (i.e., temp at less than 1 Hz). The MRI data at the 0.25 Hz condition may be an alternative to that at the discrete tempo. In the second analysis, to estimate brain activity changes for each tapping tempo, finger tapping blocks at the five tapping tempi and rest were modeled. For each participant, contrasts of each tapping tempo relative to the rest were created. Contrast-weighted parameter estimate (c*beta) maps derived from each participant were fed into the second-level random effects model analysis. We performed two-tailed one-sample t-tests to identify whole-brain positive and negative activities that were correlated with the tapping tempo during finger tapping. The final statistical threshold for significant brain activities was set at FWE $p < 0.05$ corrected for multiple comparisons at the cluster level after a height threshold of $p < 0.001$ (uncorrected), unless otherwise noted (Friston et al. 1995).

To assess correlations between brain activities and the TRF, we extracted brain activity (i.e., c*beta) at the local peak voxel within the significant clusters identified from the contrasts of interest in the parametric modulation model, using a functional VOI approach. We empirically defined four spherical VOIs with a 10-mm radius centered at the significant local peak voxel resulting from our parametric modulation analysis and previous evidence (see the Results section and Table 1). The centers of the VOIs were as follows: left M1 (MNI coordinates: x = -33, y = -22, z = 64), right cerebellar lobules VI–VII (x = 2, y = -66, z = -24), left DLPFC (x = -38, y = 30, z = 42), and left anterior cingulate cortex (ACC) (x = -10, y = 30, z = 32). Brain activity was averaged across the voxels within each VOI. To test whether tempo-modulated brain activity was associated with the TRF, we computed Pearson's skipped correlations.

Tempo-modulated effective connectivity

Using a generalized psychophysiological interaction (gPPI) analysis (McLaren et al. 2012), we identified task-evoked effective connectivity that was correlated with individual differences in the TRF. A gPPI model was created and estimated using the gPPI toolbox (https://www.nitrc.org/projects/gppi). For the seed regions for the effective connectivity analysis, we chose the following two representative VOIs based on the task-fMRI analysis: left M1 (x = -33, y = -22, z = 64) and left DLPFC (x = -38, y = 30, z = 42) with a 10-mm radius centered at the significant local peak voxel. The timeseries of voxels within each seed region were first extracted from each participant. First-level GLM, including the parametric modulator as above, was run. The gPPI

interaction term was then created by multiplying a physiological term (i.e., a deconvolved BOLD time series from the left M1 or left DLPFC) with a psychological term (i.e., a vector indicating the given tapping tempo). Subsequently, the second-level random-effects statistical analysis was conducted. We performed a group-level t-test to identify task-evoked functional connectivity associated with the tapping tempo. A height statistical threshold of $p < 0.001$ uncorrected was first applied to the whole brain. The final statistical threshold for significance was set at FWE $p < 0.05$ corrected at the cluster level, using small volume correction (svc) within each anatomically defined VOI using the Harvard-Oxford Cortical and Subcortical Structural Atlas according to the *a priori* hypothesis. For the gPPI analysis with the left M1 seed, we limited the search volume to the structurally defined right precentral gyrus, including the M1, for svc. We therefore focused on interhemispheric M1 connectivity. This hypothesis-driven analysis was based on accumulating evidence that the bilateral M1s are involved in the control of rhythmic movement (Hayashi et al. 2008; Uehara et al. 2011, 2015). Note that we will henceforth refer to this interhemispheric M1 as tempo-modulated interhemispheric M1 connectivity (IHC)

Beta estimates indicating the strength of tempo-modulated effective connectivity were obtained. We then computed Pearson's skipped correlations between the gPPI beta estimates and the TRF parameters, including *slope* and *intercept*, for each gPPI analysis.

For confirmation of the gPPI results, we verified whether the timeseries of the BOLD signals in both M1s were correlated during the tapping tasks since right M1, i.e., ipsilateral M1, activity did not reach the significant level. In order to do so, we extracted the mean time series of BOLD signals in the left and right M1s during the tapping tasks at each tempo, with a 10-mm radius centered at the significant local peak voxel (left M1: x = -33, y = -22, z = 64, right M1: x = 28, y = -18, z = 58). Subsequently, we applied Pearson's correlation analysis between each BOLD signal in the right and left M1 during the tapping tasks at each tempo for each participant and then averaged each correlation coefficient value across participants. Group-averaged correlation coefficient values were compared using a one-way repeated measures ANOVA with TAPPING TEMPO (0.25-4 Hz) as within-subjects factors, adjusted by Greenhouse-Geisser correction as the assumption of sphericity was violated. We then performed post-hoc explorations using Bonferroni correction for multiple comparisons.

Resting-state functional connectivity

Accumulating evidence has indicated that the basic architectures of task-evoked and resting-state networks are similar. That is, spontaneous brain activity (i.e., resting-state networks) contains patterns that are also seen in task-evoked or sensory-induced brain activity (Kenet et al. 2003; Luczak et al. 2009, 2013; Berkes et al. 2011). Here, we investigated whether task-evoked connectivity and resting-state connectivity are associated with similar or distinct aspects of rhythmicity control. Specifically, we hypothesized that the influence of resting-state connectivity on rhythmicity would be stronger for slow tempi, because the relevant network should experience a longer idling (i.e., resting) state during slow tempi than during fast tempi. Thus, the hypothesis was that resting-state connectivity would be more

strongly correlated with the *intercept* of the TRF than the *slope*.

Resting-state functional connectivity was computed by a VOI-to-VOI analysis, using the Conn toolbox. We defined VOIs in the bilateral M1s, left DLPFC, and left SMG according to the task-fMRI and gPPI results. For each participant, the preprocessed BOLD time series signals were extracted from all voxels within each VOI and averaged to produce mean BOLD timeseries for each VOI. The averaged BOLD time courses were used as a regressor in each participant's GLM to assess functional connectivity. To calculate resting-state connectivity between the bilateral M1s, we then calculated the temporal correlation (Pearson's *r*) between the averaged BOLD signal timeseries of predefined VOIs, followed by Fisher's z-transformation. The statistical threshold for significance was set at $p < 0.05$ FWE-corrected for multiple comparisons. Finally, we conducted Pearson's skipped correlations between the strength of the resting-state connectivity of the bilateral M1s and the left DLPFC-left SMG and the TRF.

Multiple regression analysis

The series of correlation analyses identified correlations of the *slope* and *intercept* of the TRF with tempo-modulated brain activity and connectivity, as well as resting-state connectivity in the bilateral M1 and DLPFC-SMG networks (See details in Results and Supplementary Figure 5). To clarify how these sets of variables are related to the control of tempo-dependent rhythmicity (i.e., *slope*) and discrete timing (i.e., *intercept*) when considered together, we applied a multiple regression analysis in a nonhierarchical stepwise manner, using the dependent variables identified as significant in the series of correlation analyses. The independent variable was either the *slope* or the *intercept* of the TRF. The dependent variables were tempo-modulated brain activity in the left M1 and left DLPFC (2 tempo-modulated local brain activity), tempo-modulated IHC and left DLPFC-SMG connectivity (2 tempo-modulated connectivity), resting-state IHC and left DLPFC-SMG connectivity (2 resting-state connectivity) and their interactions. These dependent variables were selected because they survived our single correlation analyses. This multiple regression analysis was implemented using the R environment (R 3.5.3 www.r-project.org).

Results

Interindividual variability in the effects of movement tempo on rhythmicity

In the behavioral analyses, we concentrated on analyzing CVs of ITIs as an index of motor rhythmicity. When averaged across participants, the CV monotonically increased as a function of the tempo (Figure 1a). Overall, faster tempi reduced rhythmicity precision, and this phenomenon is akin to a conventional behavior model known as speed-accuracy trade-off (Fitts 1954). We however noticed substantial inter-individual variability in the effects of tempo on rhythmicity, which suggests that there is complexity to model the tempo-precision trade-off relationship between tempo and rhythmicity.

The individual differences in the tempo-rhythmicity relationship were hypothesized to reflect those in latent control strategies to fit to various tapping tempi. We thus intended to model the relationship between the tempo and the accuracy, using a simple mathematical function (i.e., TRF). First, we compared which of the linear function or the quadratic function better explained the tempo-rhythmicity relationship, by referring to the RMSE in each participant. This procedure found the linear model more adequate than the quadratic model in around 80% of the participants. The group-wise mean RMSE was significantly smaller for the linear model (0.07 ± 0.09) than for the quadratic model (0.11 ± 0.09) (t=-3.34, p=0.029 by a paired t-test), supporting the linear model over the quadratic model. We thus chose the linear model as the TRF. With the linear TRF, the group-wise mean R^2 value was 0.57 ± 0.32 (standard deviation, SD) suggesting fair goodness-of-fit of the model.

Second, we analyzed the two parameters derived from the TRF to characterize individuals' tempo-rhythmicity relationship. We found considerable individual variability in both the *slope* and *intercept* of the TRF, as revealed by their broad distribution. The *slope* and *intercept* of the TRF showed a strong inverse correlation (95% confidence interval (CI) [-0.98 to -0.92], r = -0.93; Figure 1b). Namely, participants with precise motor rhythmicity at lower tempi were less precise at higher tempi (see subject A in Figure 1c for an example of a conventional tempo-precision trade-off). Conversely, participants with imprecise motor rhythmicity (a high CV) at lower tempi showed improved rhythmicity at faster tempi (see subject B in Figure 1c for an example of a paradoxical tempo-precision trade-off). The conventional and paradoxical

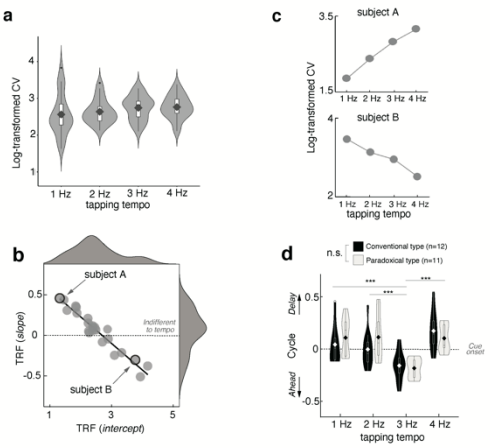

Figure 1: Behavioral results
a, Violin plots showing log-transformed CVs for ITIs in each tapping tempo. A higher value indicates more disruption of motor rhythmicity during finger tapping. The boxes indicate the interquartile ranges. Diamonds and the error bars indicate the mean and SD, respectively. The violin-shaped areas indicate data density. The black dots represent outliers. **b,** A scatterplot showing the relationship between the *slope* and *intercept* of the TRF. Marginal density plots of x-axes (top panel) and y-axes (right panel) indicate the distribution of the *intercept* and *slope* values, respectively. One dot represents data from one participant. For the y-axis, positive values indicate that rhythmicity was disrupted by the increase in tapping tempo, while negative values indicate that rhythmicity was improved by the increase in tapping tempo. For the x-axis, high values indicate imprecise rhythmicity at a slow tempo (i.e., discrete movement). **c,** Typical examples of changes in CVs across the given tapping tempi from representative participants are shown (subject A and B). **d,** Violin plots showing the degree of synchronization between each finger tap and each cue sound. A dot horizontal line depicts the auditory cue onset. A positive value indicates that finger tapping was reactively made after the cue sound. In contrast, a negative value indicates that finger tapping was proactively performed before the cue sound. The black diamonds depict the mean values of synchronization. Conventional (black bar) and paradoxical (white bar) groups were consisted of 12 and 11 participants, respectively. N.s. and three asterisks denote a no significant difference and a significant deference between tapping tempo ($p < 0.001$), respectively. Unless otherwise noted, data are plotted in the same format as Figure 1a.

tempo-precision trade-off types might not form distinct entities and rather be part of a continuous trait (Figure 1b).

Third, we further analyzed the TRF-derived parameters in relation to the cues or other behavioral data to help with the interpretations. We performed an additional data analysis to dispel concerns that the findings about the paradoxical tempo-precision trade-off resulted from a cheating strategy in some participants. That was, it was possible that participants who skipped taps to maintain the high tempo (e.g., tapped only to every two cues) would appear as the paradoxical tempo-precision trade-off type. However, we found no correlation between the number of actual taps and the CV value, making the skipping strategy unlikely (Supplementary Table 1). A more plausible strategy was that some participants might maintain rhythmicity by sacrificing synchronization between the cues and the taps. To exclude this possibility, we assessed the maintenance of the temporal synchronization as a function of tempo (Figure 1d). The participants in the main experiment were operationally classified into the conventional (n=12) and paradoxical (n=11) types according to individual median in reference to group median of the *slope* to further clarify differences in their control strategies (Supplementary Figure 1a). Both groups maintained the temporal gaps between the cues and movement at around 0.1- 0.2 cycles. Hence, the participants performed synchronized tapping as requested according to a previous study reporting that -0.25 to 0.25 cycles ahead or delay to each cue sound was acceptable for synchronized tapping (Toma et al. 2002). Meanwhile, we noticed that the participants appeared to use slightly different synchronization strategies across the tempo; they were reactive at 1, 2 and 4 Hz while proactive at 3 Hz overall. A two-way repeated measure and mixed design ANOVA with the 'group' (two levels: conventional and paradoxical) and the 'tempo' (four levels: 1, 2, 3, and 4Hz) factors revealed significant differences in the temporal synchronization (i.e., cycle) across the tapping tempi ($F_{[2.4,\ 51.4]}$=21.0, p=0.001), without the main effect of the group ($F_{[1,21]}$=0.21, p=0.64) or the interaction between the group and the tempo ($F_{[2.4,\ 51.4]}$=2.09, p=0.12). This analysis excluded the possibility that inter-individual differences in the synchronization strategy resulted in the segregation between the conventional and paradoxical types. Although the linear mode was better overall as above, a concern is that there might be a difference in the appropriate model for the two groups. For example, a quadratic model could be better suited to the paradoxical type than a linear model, so the linear model might not adequately model the behavior of the paradoxical type. To rule out this possibility, we examined the group-wise difference in the proportion of participants who showed better fitting to the linear or the quadratic model. The linear model was better than the linear model in majority of the participants for both the paradoxical group (75%) and the conventional group (83.3%) (Supplementary Figure 1b), supporting that the linear model was better regardless of the paradoxical or the conventional group.

Another question was if motor learning influenced CV through multiple blocks and sessions. The analysis indicated that the motor learning effect unlikely affected CV in response to the tapping tempo. Detailed information is shown in Supplementary Figure 2.

We confirmed the replicability of the tempo-precision tradeoff behavior, using data

obtained from additional 12 participants (Supplementary Figure 3). The CV values from 1 to 3 Hz were fitted using a linear regression model for each participant. The analytic procedures for the behavioral data were the same as that for the main dataset. The two types of rhythmicity control schemes, i.e., the conventional and paradoxical tempo-precision trade-off, were replicated in this cohort (Supplementary Figure 3c). As in our main experiment (Figure 1), a significantly negative correlation between the *intercept* and *slope* of the TRF was observed (95% CI [-0.96 to -0.14], r=-0.88) (Supplementary Figure 3b).

The relationship between tempo-modulated brain activity and rhythmicity

We analyzed: 1) how the whole brain responded to each tapping tempo (tempo-modulated brain activity), and 2) how the tempo-modulated brain activity related to the tempo-precision trade-off behavior as captured by TRF.

First, our parametric design, including a regressor (modeling five tapping tempi) along with a state model for the task blocks showed that tempo was positively correlated with activity in the left precentral gyrus, including the M1, right operculum, and right cerebellar lobules VI–VII, at a family-wise error (FWE)-corrected p-value < 0.05 (Figure 2a and b, Table 1). These findings were supported by the parameter estimates (c*beta) of task-related activity that were analyzed separately for each tempo (Figure 2c). Additionally, tempo was negatively correlated with activity in frontal regions that are related to cognition, including the left DLPFC, left ACC, and left middle frontal gyrus. The DLPFC and ACC have been reported to underlie the adaptive control of behavior with varying movement and cognitive speed (Bogacz et al. 2010; Wenzlaff et al. 2011; Vallesi et al. 2012; Weigard et al. 2019).

Second, to assess the correlations between task-induced brain activities and the *slope* and *intercept* of the TRF, we extracted brain activity (c*beta) using the following four spherical functional volumes of interest (VOIs): the left M1 (x = -33, y = -22, z = 64), right cerebellar lobules VI–VII (x = 2, y = -66, z = -24), left DLPFC (x = -38, y = 30, z = 42), and ACC (x = -10, y = 30, z = 32). The *slope* of the TRF was correlated with brain activity in the left M1 (95% CI [-0.05 to -0.76], r = -0.45) and left DLPFC (95% CI [0.05 to 0.76], r = 0.46) (Figure 3a). The *intercept* of the TRF was also correlated with brain activity in the left M1 (95% CI [0.08 to 0.62], r = 0.38) and left DLPFC (95% CI [-0.73 to -0.01], r = -0.41) (Figure 3b). There were no significant correlations between activity in the cerebellum or ACC with either the *slope* or the *intercept* (Supplementary Figure 4). To summarize, paradoxical tempo-precision trade-off behavior was accompanied by M1 activity that was responsive to the tapping tempo, whereas the conventional tempo-precision trade-off behavior was associated with less responsive M1 activity. Conversely, responsive activity in the left DLPFC was also associated with paradoxical tempo-precision trade-off behavior (precise rhythmicity at fast tempi and imprecise rhythmicity at slow tempi).

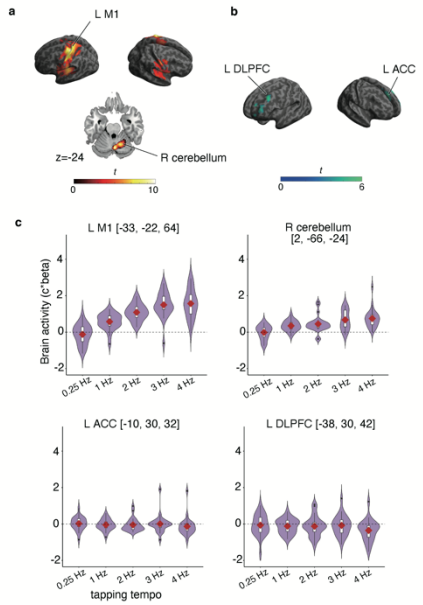

Figure 2: Brain activity that was positively (a) and negatively (b) correlated with tapping tempo

a, Positively correlated tempo-modulated brain activity was found in the left M1, and right cerebellar lobules VI–VII. **b,** Negatively correlated tempo-modulated brain activity was found in the left DLPFC and left ACC. The activity was thresholded at FWE $p < 0.05$ corrected for multiple comparisons at the cluster level. The color scales indicate the t-values. **c,** The violin plots represent the data density of brain activity at each tempo (c*beta) sampled from the VOIs in the left M1, left cerebellar lobules VI–VII, left DLPFC, and left ACC (SPM anatomy toolbox, see Table 1). The boxes indicate the interquartile range. The red diamonds and the error bars indicate the mean and SD, respectively. The black dots represent outliers. The dashed lines superimposed onto the violin plots represent the baseline (i.e., brain activity during the rest block).

The relationship between rhythmicity and tempo-modulated functional connectivity

We analyzed: 1) how brain functional connectivity was modified in response to tapping tempo (tempo-modulated functional connectivity) and 2) how tempo-modulated functional connectivity was related to the tempo-precision trade-off behavior (correlation with TRF parameters).

For the gPPI analysis with the left M1 seed, we found that tapping tempo was correlated with the interhemispheric connectivity between the left and the right M1 (x = 28, y = -18, z = 58; t = 4.79; svc-corrected p = 0.009; Figure 4a). The PPI values (beta value) obtained from each tapping tempo showed that the effective connectivity between both M1s was increased as a function of the tapping tempo (Figure 4b). This result indicated that, although the right M1 did not show correlated activity with the tapping tempo in the whole-brain correlation analysis (Figure 2a), both M1s showed synchronized fluctuation of activity during rhythmic movement. For confirmation, we performed a correlation analysis of the timeseries of BOLD signals sampled from both M1s and verified that the change of activity was correlated between bilateral M1s in a tempo-dependent manner. The details of this confirmation analysis are described in Supplementary information 1. This analysis indicates that contralateral M1 activity was positively correlated with ipsilateral M1 activity during rhythmic movement even though there was no significant task-related activity in

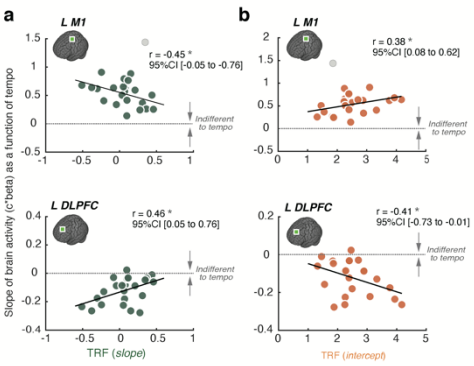

Figure 3: Correlations between tempo-modulated brain activity and TRF parameters

Relationships between tempo-modulated brain activity and the two TRF parameters, *slope* (**a**) and *intercept* (**b**). **a**, A positive TRF *slope* (abscissa) indicates that rhythmicity was disrupted by the increase in tapping tempo, and that of the ordinate indicates that brain activity was increased as a function of tapping tempi. **b**, A higher value of the *intercept* indicates imprecise rhythmicity at a slow tempo (i.e., near-discrete movement). Correlations were considered significant if the 95% CI did not include zero. *: significant correlation. One dot represents data from one participant. An outlier is displayed as a gray dot.

the ipsilateral M1. In sum, we assume that ipsilateral M1 activity can show task-correlated fluctuation in a limited range of an inhibition-excitation cycle. A correlation analysis revealed that the tempo-modulated IHC was negatively correlated with the TRF *slope* (95% CI [-0.75 to -0.21], r = -0.53; Figure 4c), but not with the TRF *intercept* (95% CI [-0.02 to 0.46], r = 0.23) (Figure 4d). Other than M1s, the whole brain gPPI analysis found a trend in the right superior temporal gyrus (STG) (MNI coordinates x = 56, y = -28, z = 2) at the uncorrected level (p<0.001). However, because we did not have an *a priori* hypothesis on the role of STG in the control of motor rhythmicity, we did not apply svc in accordance with the guidelines for reporting an fMRI study (Poldrack 2007; Poldrack et al. 2008). The alternative hypothesis to the IHC hypothesis was that tempo-modulated left DLPFC-left SMG connectivity might be related to a cognitive aspect of motor rhythmicity adjustment. For the gPPI analysis with the left DLPFC seed, we limited the search volume to the structurally defined left SMG for svc. However, we failed to find tempo-modulation of the left DLPFC-left SMG connectivity (x = -56, y = -48, z = 40; t = 3.77; svc-corrected p = 0.10). Neither the *slope* nor the *intercept* was correlated with left DLPFC-left SMG connectivity (*slope*: 95% CI [-0.39 to 0.35], r = -0.004; *intercept*: 95% CI [-0.25 to 0.48], r = 0.11). The tempo-modulated effective connectivity analyses showed that IHC, but not fronto-parietal connectivity, was modulated by the tapping tempo. Furthermore, we found a relationship between tempo-modulated IHC and the *slope* of the TRF, which indicates that individuals with responsive tempo-modulated IHC exhibited precise rhythmicity at fast tempi.

The relationship between resting-state functional connectivity and rhythmicity

In the present study, we wanted to identify how the resting-state functional connectivity was involved in the parameter captured by TRF because the resting-state networks likely contain patterns encompassed by task-evoked brain activity (Kenet et al. 2003; Luczak et al. 2009, 2013; Berkes et al. 2011).

Using a VOI-to-VOI approach, we found significant resting-state functional connectivity between the bilateral M1s (i.e., resting-state IHC) (FWE-corrected p = 0.002) and between the left DLPFC and left SMG (FWE-corrected p

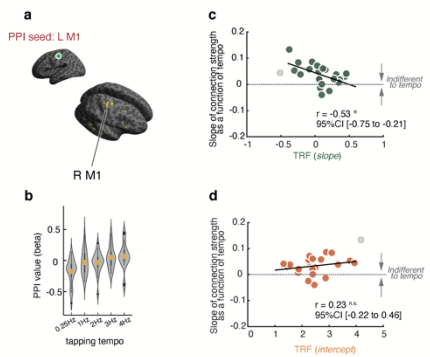

Figure 4: Correlations between tempo-modulated M1 IHC and TRF parameters

a, The left M1 activity (seed) was correlated with right M1 activity in a tempo-dependent manner (svc within an anatomical mask). For display purposes, activated regions were thresholded at p < 0.001 uncorrected. **b**, The violin plots represent the data density of the PPI values (beta value) sampled from the VOIs in the right M1. The boxes indicate the interquartile range. The orange-diamonds and the error bars indicate the mean and SD, respectively. The black dots represent outliers. **c,** The scatterplot depicts the correlation between tempo-modulated IHC and the *slope* of the TRF. **d,** As shown in the scatterplot, there was no correlation between tempo-modulated IHC and the TRF *intercept*. Correlations were considered significant if the 95% CI did not include zero. n.s.: no significant correlation. *: significant correlation. Each dot represents data from one participant. Outliers are displayed as a gray dot.

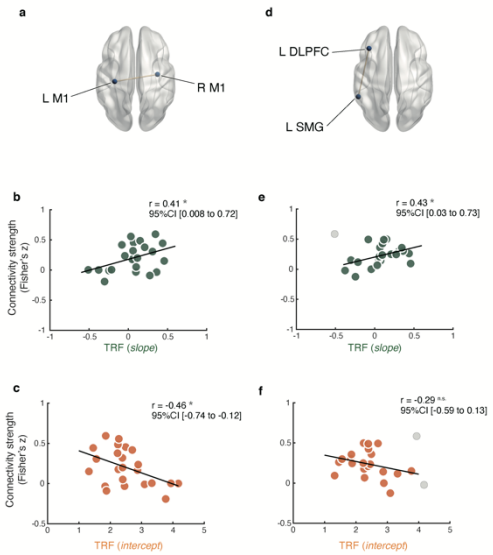

Figure 5: Correlations between resting-state connectivity and TRF parameters

a, The left M1 was significantly interconnected with the right M1 at rest. **b,** Strength of the resting-state interhemispheric M1 connectivity was significantly positively correlated with the *slope* of the TRF. **c,** The strength of the resting-state interhemispheric M1 connectivity was significantly negatively correlated with the *intercept* of the TRF. **d,** The left DLPFC was significantly interconnected with the left SMG at rest. **e,** The resting-state connectivity between the left DLPFC and left SMG was significantly positively correlated with the *slope* of the TRF. **f,** The strength of the resting-state connectivity of the left DLPFC-left SMG was not correlated with the *intercept* of the TRF. Pearson's correlation was applied using a bootstrapped method. Correlations were considered significant if the 95% CI did not include zero. An asterisk indicates a significant correlation. One dot represents data from one participant. Outliers are displayed as a gray dot.

= 0.002) based on the *a priori* hypothesis. The bootstrapped correlation analyses revealed that resting-state IHC was positively correlated with the *slope* (95% CI [0.008 to 0.72], r = 0.41), and negatively correlated with the *intercept* of the TRF (95% CI [-0.74 to -0.12], r = -0.46) (Figure 5a, b, and c). The almost identical strength of correlation with slope and with intercept may seem inconsistent with our hypothesis that resting-state connectivity would be more involved in slow tempi, predicting a higher correlation between IHC and the *intercept* of the TRF than the *slope* of the TRF. Conversely, resting-state left DLPFC-SMG connectivity was positively correlated with the *slope* (95% CI [0.03 to 0.73], r = 0.43), but not with the *intercept* (95% CI [-0.59 to 0.13], r = 0.29) (Figure 5d, e, and f).

We found that resting-state functional connectivity contained information on the control of motor rhythmicity, even though resting-state fMRI data were acquired before the task-fMRI data. We also found that resting-state IHC was associated with both TRF parameters, whereas the tempo-modulated IHC was correlated only with the *slope* of the TRF. Individuals who had a stronger resting-state IHC had better rhythmicity at slow tempi close to the discrete movement. Conversely, individuals who had weaker resting-state IHC had better rhythmicity at faster tapping tempi. Resting-state left DLPFC-SMG connectivity was also associated with tempo-dependent rhythmicity. Individuals

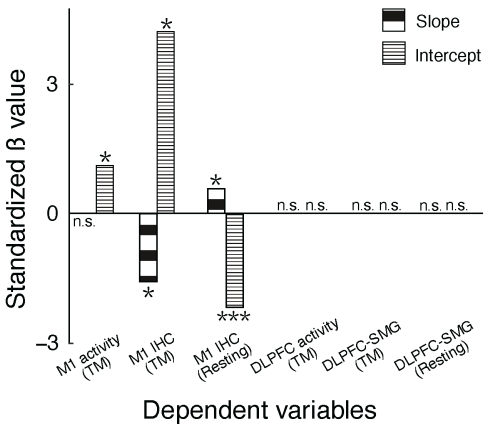

Figure 6: Summary of multiple regression analyses

The standardized β-values obtained from the multiple regression analyses for the predictions of the *slope* and the *intercept* models are plotted. Asterisks indicate a significant dependent variable (*p < 0.05, ***p < 0.001). n.s.: no significant difference; IHC: interhemispheric connectivity between motor cortices; TM: tempo-modulated; Resting: resting-state connectivity.

who had weaker resting-state left DLPFC-SMG connectivity showed a higher precision of tempo-dependent rhythmicity at faster tapping tempi.

Multiple regression analysis

Finally, we aimed at clarifying how the tempo-precision trade-off behavior (TRF) was coded within the interplay of these neural features. To address this issue, we performed multiple regression analyses.

The variance inflation value (VIF) for the dependent variables was less than 1.5 (accepted VIF < 5.0), which is suggestive of no multicollinearity between the tempo-modulated activity, tempo-modulated connectivity, and resting-state connectivity. Figure 6 shows the summary of the multiple regression analyses. The best fit model for the *slope* of the TRF ($F_{4,18}$ = 5.42, p = 0.004, adjusted R^2 = 0.44 for the model) included the tempo-modulated IHC (standardized β = -1.58, p = 0.02) and the resting-state IHC (standardized β = 0.57, p = 0.02). The best fit model for the *intercept* of the TRF ($F_{3,19}$ = 6.55, p = 0.003, adjusted R^2 = 0.43) included the tempo-modulated IHC (standardized β = 4.22, p = 0.03), resting-state IHC (standardized β = -2.18, p = 0.001), and tempo-modulated left M1 activity (standardized β = 1.11, p = 0.03). Tempo-modulated and resting-state functional connectivity of the left DLPFC-left SMG and brain activity in the left DLPFC were not included in the best fit model.

The results were not completely consistent between the single correlation analyses and the multiple regression analyses, especially in terms of prefrontal activity and DLPFC-SMG connectivity. Moreover, while the correlation analyses did not detect a relationship between the tempo-modulated IHC and TRF *intercept*, the multiple regression analysis found that tempo-modulated IHC had a meaningful impact on the TRF *intercept*. It is possible that tempo-modulated IHC may act as a suppressor variable when treated together with other variables; such a suppressor variable may not yield strong correlations in single correlation analysis, but can serve as a meaningful independent variable with the addition of other dependent variables (Meyers et al. 2017). Indeed, the multiple regression analysis showed that tempo-modulated M1 activity and tempo-modulated and resting-state IHC were the most influential explanatory factors of individual differences in tempo-dependent rhythmicity.

Discussion

We propose tempo-dependent rhythmicity as a new type of tempo-precision trade-off phenomenon and provide novel evidence for the two types of neural-behavioral coupling for rhythmicity control. Although rhythmicity became imprecise with fast tempi overall, individuals substantially differed in their adjustment strategy of rhythmicity from slower to faster tempi. We characterized these interindividual differences according to the control mechanisms of tempo-dependent rhythmic movement using two parameters of the TRF, namely, the *slope* and the *intercept.* The *slope* reflected tempo-dependent rhythmicity, and the *intercept* is closely related to the timing control of discrete movement, i.e., discrete timing. To uncover the neural correlates of these two behavioral repertoires, we examined task-related brain activity, task-related effective connectivity, and resting-state functional connectivity,

especially of the bilateral M1 and the left fronto-parietal network. We found that the tempo-modulated and resting-state IHC of the bilateral M1, rather than fronto-parietal connectivity, played a pivotal role in the control mechanisms underlying tempo-dependent rhythmicity.

The analysis of individual variabilities in rhythmicity control using the TRF concept revealed two behavioral extremes: conventional and paradoxical tempo-precision trade-off types. The conventional type appears to outnumber the paradoxical type (Figure 1b and Supplementary Figure 3b). In general, increasing tapping tempo sacrifices motor rhythmicity. In the conventional type (subject A and C in Figure 1c and Supplementary Figure 3c, respectively), rhythmicity decreased with a faster tempo (i.e., positive *slope*), despite precise rhythmicity during slower tempi (i.e., low *intercept*). In the paradoxical type (e.g., subjects B and D in Figure 1c and Supplementary Figure 3c, respectively), rhythmicity became more precise with faster tempi, yielding a high *intercept* and negative *slope*. In essence, the *slope* and the *intercept* are independent in the linear regression scheme. However, we found a strong negative correlation between the *slope* and the *intercept* of the TRF (Figure 1b and Supplementary Figure 3b), which implies that there is a link between tempo-dependent rhythmicity and discrete timing control. Individuals with precise control of discrete timing were not good at maintaining tempo-dependent rhythmicity, whereas individuals with imprecise control of discrete timing were good at maintaining tempo-dependent rhythmicity at faster tempi. It remains a matter of debate how rhythmic and discrete movements are controlled by the central nervous system (Smits-Engelsman et al. 2002; Hogan and Sternad 2007; Hira et al. 2015; Wiegel et al. 2020). It is also unclear which neural entities are involved in rhythmic and discrete movements, or how cortical areas interact with the CPG during rhythmic movements from slow to fast tempi. The present findings contribute in part to the settlement of this argument. To our knowledge, this is the first study to investigate which brain areas, networks, and neural states (responsiveness to the tempo) underlie the precision of tempo-dependent rhythmicity. The multiple regression analysis revealed that the tempo-modulated and resting-state IHC contributed to the prediction of both the *slope* and the *intercept* of the TRF. Furthermore, we provide new evidence that the responsivity of M1 activity and IHC are substantially different between near-discrete timing (i.e., *intercept*) and tempo-dependent rhythmicity (i.e., *slope*). Although we confirmed that DLPFC activity and fronto-parietal connectivity were involved in rhythmicity control to some extent, their contribution was only minor when we considered the contribution of motor activity/connectivity together. Hence, the motor systems, especially the IHC between M1s, could influence motor rhythmicity control more than cognitive systems assigned to the fronto-parietal regions.

Accumulating evidence has supported the active roles of IHC in the control of motor rhythmicity. A virtual lesion study using repetitive transcranial magnetic stimulation revealed that ipsilateral M1 stimulation induced timing errors while performing repetitive sequential finger movements (Chen et al. 1997). This finding supports the idea that the ipsilateral M1 is involved in the processing of motor programs controlling rhythmic actions, presumably through IHC. Moreover, interhemispheric inhi-

bition between the contralateral and ipsilateral M1s contributes to the evenness of repetitive actions (Kuo et al. 2019). Likewise, our results support these human neuroimaging studies. During a unilateral motor action, the ipsilateral M1 showed task-specific activity changes that were not simply a copy of the contralateral M1 activity. The ipsilateral M1 has been reported to be involved more in motor planning than in motor execution during a unilateral motor action (Diedrichsen et al. 2013; Berlot et al. 2019). Together, this evidence indicates that cooperative interactions between both M1s, which correspond to IHC in this study, are likely to play active roles in the control of rhythmicity.

The correlation of bilateral M1 activities at rest (resting-state connectivity) has been widely accepted and reproduced (Biswal et al. 1995; van den Heuvel and Pol 2010). Although significant task-related activity was observed in the contralateral M1 only, our gPPI analysis yielded that the bilateral M1s showed concerted changes in activity during rhythmic movement at all tempi (Figures 4a and b). This observation was corroborated by the BOLD time-series correlation between both M1s (Supplementary information 1). This analysis indicates that contralateral M1 activity was positively correlated with ipsilateral M1 activity during rhythmic movement even though there was no significant task-related activity in the ipsilateral M1. It has been thought that ipsilateral M1 activity is suppressed by interhemispheric inhibition from the contralateral M1 while performing a unilateral movement (Ferbert et al. 1992; Uehara et al. 2014). However, in the present study, ipsilateral M1 activity was not simply suppressed by interhemispheric inhibition from the contralateral M1. A plausible explanation comes from previous TMS studies in humans, showing that interhemispheric connection from the opposite M1 inhibited short-interval intracortical inhibition (SICI). The inhibition of SICI leads to the disinhibition of the ipsilateral M1, which could produce an inhibition-excitation cycle together with interhemispheric inhibition. We therefore assume that ipsilateral M1 activity can show task-correlated fluctuation in a limited range allowed by the combination of interhemispheric inhibition and disinhibition of SICI.

In the present study, we identified two neural-behavioral coupling traits for motor rhythmicity control: the responsive brain network-paradoxical trade-off type and the indifferent brain network-conventional trade-off type. Identification of these types could help elucidate the individual differences between tempo-dependent rhythmicity and discrete timing. The responsive network type was defined as a strong tempo-modulated IHC accompanied by a weak resting-state IHC. The weak resting-state IHC suggested temporarily sparse synchronization of networks at the baseline level. The strong tempo-modulated IHC implied a responsive network to meet the contextual demand of a faster tempo. These two properties are akin to those of tunable sparse network coding (Olshausen and Field 2004; Spanne and Jörntell 2015). We found that flexible modulation of brain activity and connectivity allowed individuals to maintain rhythmicity in the face of contextual demands. This finding is consistent with the relatively recent concept of greater modularity of brain networks, or sparser connectivity for more flexible behavior (Bassett et al. 2011; Bassett and Mattar 2017; Mattar et al. 2018). Namely, densely interconnected modules may fail to respond to the increasing demands of incoming stimuli, while sparsely interconnected modules may enable better be-

havioral adaptation to a changing environment. Previous work has shown that flexible brain networks can enhance learning, because they can generate a new neural activity pattern to acquire a new behavior (Bassett et al. 2011). Similarly, the responsive network type would supposedly allow flexible adjustment of behavior to faster tapping tempi, leading to better control of tempo-dependent rhythmicity. Conversely, the indifferent network type would not be able to increase the network functionality well enough to meet the requirements of both the number of finger taps and the rhythmicity under the larger demands of faster tempi.

Our results indicated that the responsive network type was not always advantageous, because it was not accompanied by good timing control at slow tempi (i.e., discrete timing). Conversely, individuals who adopted the indifferent network type were able to produce precise timing at the slow tempi. The indifferent network type was characterized by an IHC that was unresponsive to changes in tempo and a stronger resting-state IHC (Figures 4d and 5c). These observations can be explained in two ways. First, stronger resting-state IHC likely indicates that the bilateral M1s were well interconnected at baseline, and that the degree of connectivity may have been close to ceiling level. If this is the case, there is less possibility for IHC to be enhanced in the face of increased tempo demands. Alternatively, the dense connections of the IHC may be unresponsive to increasing tempi because dense neural coding may suffer from cross-talk (i.e., collisions) across neurons (Olshausen and Field 2004; Spanne and Jörntell 2015). Thus, the indifferent network type might not be able to flexibly modulate the strength of the IHC to meet the contextual demand of the tapping tempo. However, the indifferent network type may not be always disadvantageous; we also found that this stable or consistent connectivity likely helps to achieve precise control of discrete timing.

Notably, even though the indifferent network type was able to maintain the necessary number of finger taps for each given tempo, brain activity and the strength of the network were almost unchanged, despite the changing tempi (Supplementary Table 1). Here, it should be noted that 1) the number of finger taps *per se* did not influence changes in M1 activity or IHC, and 2) the unchanged activity and connectivity across the tempi co-existed with a decline in motor rhythmicity for fast tempi. Both points further our basic understanding of the relationship between rhythmic movements and the hierarchically organized cortical and subcortical systems. In the present study, the responsive and indifferent types of IHCs at least partly explained the individual differences in control mechanisms of tempo-dependent rhythmicity and discrete timing. An open question is whether semi-automatic rhythm generators such as the CPG are involved in tempo-related rhythmicity control. The CPG is thought to generate periodic-rhythmic activity automatically during rhythmic movement (Eve Marder and Dirk Bucher 2001; Grillner 2006; Harris-Warrick 2011). We speculate that this CPG-based automatic control could serve as the generator for basic rhythmicity during finger tapping. This would explain why the indifferent network type can produce the required number of taps at faster tempi without recruiting the M1 or IHC to such a great extent. Indeed, this was achieved at the cost of poor rhythmicity. Our results suggest that involvement of the bilateral M1 may be more important for precise control of externally triggered rhythmicity than for the

mere production of rhythmic tapping at faster tempi. Recently, Cadena-Valencia and colleagues reported rhythmicity in gamma-band bursts in the motor area during entrainment to external tempi in non-human primates, and they used the timing of gamma bursts to predict whether responses would be ahead or behind a given tempo (Cadena-Valencia et al. 2018).

The present study has potential limitations. The model comparison found a linear function between CVs and tapping tempo better explained each individual's data than the quadratic function. There should be many non-linearities in the motor system. Indeed, we might have been able to find an optimal frequency for each individual as a vertex of a quadratic function if wider ranges of tapping tempo had been covered (e.g., less than 0.25 Hz and higher than 4 Hz). By realizing this study limitation, our future study will extend the present finding to explore non-linearity of the tempo-precision relationship, using different experimental designs. In addition, we estimated a parameter representing the discrete timing control, using the intercept derived from the linear regression model. Based on this estimation and novel findings in this study, our future study will work out a new experimental design and a mathematical model about how to extract information of the rhythmicity and the discrete timing control comprehensively.

We employed task-fMRI investigation with the block-design paradigm. Hence, the number of the finger tapping varied depending on the tapping tempi. This is a technical limitation of task-fMRI studies using task/stimulus rates across blocks. However, it was unlikely that brain activity and networks simply reflected the differences in the number of taps. The participants with the indifferent network type showed almost unchanged brain activity and connectivity even though they maintain the necessary number of finger taps for all tempi. Together, this finding suggests that control strategies of rhythmic movement rather than the number of movements affect changes in brain activity or connectivity.

Conclusion

We identified two neural-behavioral coupling types for rhythmicity control, namely, a combination of the paradoxical tempo-precision trade-off and the responsive networks, and that of the conventional tempo-precision trade-off and the indifferent network. In particular, individual differences in the responsiveness of IHC may underlie individual variation of control strategies of tempo-dependent rhythmicity under fast tempo demands. The fact that the responsive IHC was coupled with weak resting-state IHC can be explained by the concept of tunable sparsely coded connectivity. The present tempo-rhythmicity trade-off paradigm opens new avenues for studying the foundation of skillful finger movements in humans, some of whom are tuned to slow and some to fast tempi.

Funding

This study was supported by a postdoctoral research fellowship from the Japan Society for the Promotion Science (JSPS) to KU (14J00119) and HT (17J05927), and by the JSPS KAKENHI (19K20103) to KU and by the Japan Agency for Medical Research and Development (JP19dm0207070, JP19dm0307003), JSPS KAKENHI (19H05726, 19H03536), Japan Science and Technology Agency, CREST, (JPMJFR206G) and National Center of Neurology and Psychiatry Intramural grant (30-4) to TH.

Acknowledgments

We thank laboratory members for their help with data collection.

Conflicts Interest Statement

The authors declare that no competing interests exist.

Author Contributions

KU and TH designed the experiments and wrote the manuscript; KU and HT performed data collection and analyzed the data. All authors read and approved the final version of manuscript.

References

Aso K, Hanakawa T, Aso T, Fukuyama H. 2010. Cerebro-cerebellar Interactions Underlying Temporal Information Processing. J Cogn Neurosci. 22:2913–2925.

Bassett DS, Mattar MG. 2017. A Network Neuroscience of Human Learning: Potential to Inform Quantitative Theories of Brain and Behavior. Trends Cogn Sci. 21:250–264.

Bassett DS, Wymbs NF, Porter MA, Mucha PJ, Carlson JM, Grafton ST. 2011. Dynamic reconfiguration of human brain networks during learning. Proc Natl Acad Sci U S A. 108:7641–7646.

Beckmann CF, DeLuca M, Devlin JT, Smith SM. 2005. Investigations into resting-state connectivity using independent component analysis. Philos Trans R Soc B Biol Sci. 360:1001–1013.

Behzadi Y, Restom K, Liau J, Liu T. 2007. A Component Based Noise Correction Method (CompCor) for BOLD and Perfusion Based fMRI. Neuroimage. 37:90–101.

Berkes P, Orbán G, Lengyel M, Fiser J. 2011. Spontaneous cortical activity reveals hallmarks of an optimal internal model of the environment. Science. 331:83–88.

Berlot E, Prichard G, O'Reilly J, Ejaz N, Diedrichsen J. 2019. Ipsilateral finger representations in the sensorimotor cortex are driven by active movement processes, not passive sensory input. J Neurophysiol. 121:418–426.

Biswal B, Yetkin FZ, Haughton VM, Hyde JS. 1995. Functional Connectivity in the Motor Cortex of Resting. Magn Reson Med. 34:537–541.

Bogacz R, Wagenmakers EJ, Forstmann BU, Nieuwenhuis S. 2010. The neural basis of the speed-accuracy tradeoff. Trends Neurosci. 33:10–16.

Cadena-Valencia J, García-Garibay O, Merchant H, Jazayeri M, de Lafuente V. 2018. Entrainment and maintenance of an internal metronome in supplementary motor area. Elife. 7:1–23.

Chen R, Gerloff C, Hallett M, Cohen LG. 1997. Involvement of the ipsilateral motor cortex in finger movements of different complexities. Ann Neurol. 41:247–254.

Dayan E, Cohen LG. 2011. Neuroplasticity subserving motor skill learning. Neuron. 72:443–454.

Degallier S, Ijspeert A. 2010. Modeling discrete and rhythmic movements through motor primitives: A review. Biol Cybern. 103:319–338.

Diedrichsen J, Wiestler T, Krakauer JW. 2013. Two distinct ipsilateral cortical representations for individuated finger movements. Cereb Cortex. 23:1362–1377.

Eickhoff SB, Stephan KE, Mohlberg H, Grefkes C, Fink GR, Amunts K, Zilles K. 2005. A new SPM toolbox for combining probabilistic cytoarchitectonic maps and functional imaging data. Neuroimage. 25:1325–1335.

Eve Marder, Dirk Bucher. 2001. Central pattern generators and the control of rhythmic movements. Curr Biol. 11: R986–R996.

Ferbert A, Priori A, Rothwell J, Day B, Colebatch J, Marsden C. 1992. Interhemispheric inhibition of the human motor cortex. J Physiol Physiol. 453:525–546.

Fitts PM. 1954. The information capacity of the human motor system in controlling the amplitude of movement. J Exp Psychol. 47:381–391.

Friston KJ, Holmes AP, Worsley KJ, Poline J-B, Frith CD, Frackowiak RS. 1995. Statistical parametric maps in functional imaging: a general linear model approach. Hum Brain Mapp. 2:189–210.

Fujiwara Y, Matsumoto R, Nakae T, Usami K, Matsuhashi M, Kikuchi T, Yoshida K, Kunieda T, Miyamoto S, Mima T, Ikeda A, Osu R. 2017. Neural pattern similarity between contra- and ipsilateral movements in high-frequency band of human electrocorticograms. Neuroimage. 147:302–313.

Furuya S, Uehara K, Sakamoto T, Hanakawa T. 2018. Aberrant cortical excitability reflects the loss of hand dexterity in musician's dystonia. J Physiol. 596:2397–2411.

Grahn JA, Schuit D. 2012. Individual differences in rhythmic ability: Behavioral and neuroimaging investigations. Psychomusicology Music Mind, Brain. 22:105–121.

Griffanti L, Salimi-Khorshidi G, Beckmann CF, Auerbach EJ, Douaud G, Sexton CE, Zsoldos E, Ebmeier KP, Filippini N, Mackay CE, Moeller S, Xu J, Yacoub E, Baselli G, Ugurbil K, Miller KL, Smith SM. 2014. ICA-based artefact removal and accelerated fMRI acquisition for improved resting state network imaging. Neuroimage. 95:232–247.

Grillner S. 2006. Biological Pattern Generation: The Cellular and Computational Logic of Networks in Motion. Neuron. 52:751–766.

Hanakawa T, Goldfine AM, Hallett M. 2017. A Common Function of Basal Ganglia-Cortical Circuits Subserving Speed in Both Motor and Cognitive Domains. Eneuro. 0200-17.

Harris-Warrick RM. 2011. Neuromodulation and flexibility in Central Pattern Generator networks. Curr Opin Neurobiol. 21:685–692.

Hayashi MJ, Ditye T, Harada T, Hashiguchi M, Sadato N, Carlson S, Walsh V, Kanai R. 2015. Time Adaptation Shows Duration Selectivity in the Human Parietal Cortex. PLoS Biol. 13:1–27.

Hayashi MJ, Saito DN, Aramaki Y, Asai T, Fujibayashi Y, Sadato N. 2008. Hemispheric Asymmetry of Frequency- Dependent Suppression in the Ipsilateral Primary Motor Cortex During Finger Movement: A Functional Magnetic Resonance Imaging Study. Cereb Cortex. 18:2932–2940.

Hira R, Terada SI, Kondo M, Matsuzaki M. 2015. Distinct functional modules for discrete and rhythmic forelimb movements in the mouse motor cortex. J Neurosci. 35:13311–13322.

Hogan N, Sternad D. 2007. On rhythmic and discrete movements: Reflections, definitions and implications for motor control. Exp Brain Res. 181:13–30.

Ikegami T, Hirashima M, Taga G, Nozaki D. 2010. Asymmetric transfer of visuomotor learning between discrete and rhythmic movements. J Neurosci. 30:4515–4521.

Iwama S, Tsuchimoto S, Hayashi M, Mizuguchi N, Ushiba J. 2020. Scalp electroencephalograms over ipsilateral sensorimotor cortex reflect contraction patterns of unilateral finger muscles. Neuroimage. 222:117249.

Jones CRG, Rosenkranz K, Rothwell JC, Jahanshahi M. 2004. The right dorsolateral prefrontal cortex is essential in time reproduction: An investigation with repetitive transcranial magnetic stimulation. Exp Brain Res. 158:366–372.

Kelly RE, Alexopoulos GS, Wang Z, Gunning FM, Murphy CF, Morimoto SS, Kanellopoulos D, Jia Z, Lim KO, Hoptman MJ. 2010. Visual inspection of independent components: Defining a procedure for artifact removal from fMRI data. J Neurosci Methods. 189:233–245.

Kenet T, Bibitchkov D, Tsodyks M, Grinvald A, Arieli A. 2003. Spontaneously emerging cortical representations of visual attributes. Nature. 425:954–956.

Kita K, Furuya S, Osu R, Sakamoto T, Hanakawa T. 2021. Aberrant Cerebello-Cortical Connectivity in Pianists With Focal Task-Specific Dystonia. Cereb Cortex. 1–11.

Kita K, Rokicki J, Furuya S, Sakamoto T, Hanakawa T. 2018. Resting-state basal ganglia network codes a motor musical skill and its disruption due to dystonia. Mov Disord. 33:1472–1480.
Koch G, Oliveri M, Torriero S, Salerno S, Gerfo E Lo, Caltagirone C. 2007. Repetitive TMS of cerebellum interferes with millisecond time processing. Exp Brain Res. 179:291–299.
Konoike N, Kotozaki Y, Jeong H, Miyazaki A, Sakaki K, Shinada T, Sugiura M, Kawashima R, Nakamura K. 2015. Temporal and motor representation of rhythm in fronto-parietal cortical areas: An fMRI study. PLoS One. 10:1–19.
Kuo YL, Kutch JJ, Fisher BE. 2019. Relationship between Interhemispheric Inhibition and Dexterous Hand Performance in Musicians and Non-musicians. Sci Rep. 9:1–10.
Luczak A, Bartho P, Harris KD. 2013. Gating of Sensory Input by Spontaneous Cortical Activity. J Neurosci. 33:1684–1695.
Luczak A, Barthó P, Harris KD. 2009. Spontaneous Events Outline the Realm of Possible Sensory Responses in Neocortical Populations. Neuron. 62:413–425.
Mattar MG, Wymbs NF, Bock AS, Aguirre GK, Grafton ST, Bassett DS. 2018. Predicting future learning from baseline network architecture. Neuroimage. 172:107–117.
McLaren DG, Ries ML, Xu G, Johnson SC. 2012. A generalized form of context-dependent psychophysiological interactions (gPPI): A comparison to standard approaches. Neuroimage. 61:1277–1286.
Meyers LS, Glenn G, Guarino AJ. 2017. Multiple Regression. In: Applied Multivariate Research Design and Interpretation. SAGE Publications, Inc. p. 147–196.
Oldfield RC. 1971. The assessment and analysis of handedness: The Edinburgh inventory. Neuropsychologia. 9:97–113.
Olshausen BA, Field DJ. 2004. Sparse coding of sensory inputs. Curr Opin Neurobiol. 14:481–487.
Pernet CR, Wilcox R, Rousselet GA. 2013. Robust correlation analyses: false positive and power validation using a new open source Matlab toolbox. Front Psychol. 3:1–18.
Pflug A, Gompf F, Muthuraman M, Groppa S, Kell CA. 2019. Differential contributions of the two human cerebral hemispheres to action timing. Elife. 8:1–26.
Poldrack RA. 2007. Region of interest analysis for fMRI. Soc Cogn Affect Neurosci. 2:67–70.
Poldrack RA, Fletcher PC, Henson RN, Worsley KJ, Brett M, Nichols TE. 2008. Guidelines for reporting an fMRI study. Neuroimage. 40:409–414.
Power JD, Barnes KA, Snyder AZ, Schlaggar BL, Petersen SE. 2012. Spurious but systematic correlations in functional connectivity MRI networks arise from subject motion. Neuroimage. 59:2142–2154.
Reep HB, Rebercca D. 2007. Tapping to a Very Slow Beat: A Comparison of Musicians and Nonmusicians. Music Perceputions. 24:367–376.
Reis J, Schambra HM, Cohen LG, Buch ER, Fritsch B, Zarahn E, Celnik PA, Krakauer JW. 2009. Noninvasive cortical stimulation enhances motor skill acquisition over multiple days through an effect on consolidation. Proc Natl Acad Sci U S A. 106:1590–1595.
Sadato N, Ibañez V, Campbell G, Deiber M-P, Le Bihan D, Hallett M. 1997. Frequency-Dependent Changes of Regional Cerebral Blood Flow During Finger Movements: Functional MRI Compared to PET. J Cereb Blood Flow Metab. 670–679.
Sadato N, Ibañez V, Deiber MP, Campbell G, Leonardo M, Hallett M. 1996. Frequency-dependent changes of regional cerebral blood flow during finger movements. J Cereb Blood Flow Metab. 16:23–33.
Salimi-Khorshidi G, Douaud G, Beckmann CF, Glasser MF, Griffanti L, Smith SM. 2014. Automatic denoising of functional MRI data: combining independent component analysis and hierarchical fusion of classifiers. Neuroimage. 90:449–468.
Schaal NK, Pollok B, Banissy MJ. 2017. Hemispheric differences between left and right supramarginal gyrus for pitch and rhythm memory. Sci Rep. 7:1–6.
Schaal S, Sternad D, Osu R, Kawato M. 2004. Rhythmic arm movement is not discrete. Nat Neurosci. 7:1137–1145.
Shmuelof L, Krakauer JW, Mazzoni P. 2012. How is a motor skill learned? Change and invariance at the levels of task success and trajectory control. J Neurophysiol. 108:578–594.
Smits-Engelsman B, Van Galen G, Duysens J. 2002. The breakdown of Fitts' law in rapid, reciprocal aiming movements. Exp Brain Res. 145:222–230.
Spanne A, Jörntell H. 2015. Questioning the role of sparse coding in the brain. Trends Neurosci. 38:417–427.
Togo H, Rokicki J, Yoshinaga K, Hisatsune T, Matsuda H, Haga N, Hanakawa T. 2017. Effects of field-map distortion correction on resting state functional connectivity MRI. Front Neurosci. 11:1–10.
Toma K, Mima T, Matsuoka T, Gerloff C, Ohnishi T, Koshy B, Andres F, Hallett M. 2002. Movement rate effect on activation and functional coupling of motor cortical areas. J Neurophysiol. 88:3377–3385.
Uehara K, Coxon JP, Byblow WD. 2015. Transcranial Direct Current Stimulation Improves Ipsilateral Selective Muscle Activation in a Frequency Dependent Manner. PLoS One. 10:e01222434.
Uehara K, Morishita T, Funase K. 2011. Excitability changes in the ipsilateral primary motor cortex during rhythmic contraction of finger muscles. Neurosci Lett. 488:22–25.
Uehara K, Morishita T, Kubota S, Funase K. 2013. Neural mechanisms underlying the changes in ipsilateral primary motor cortex excitability during unilateral rhythmic muscle contraction. Behav Brain Res. 240:33–45.
Uehara K, Morishita T, Kubota S, Hirano M, Funase K. 2014. Functional difference in short- and long-latency interhemispheric inhibitions from active to resting hemisphere during a unilateral muscle contraction. J Neurophysiol. 111:17–25.
Vallesi A, Mcintosh AR, Crescentini C, Stuss DT. 2012. fMRI investigation of speed-accuracy strategy switching. Hum Brain Mapp. 33:1677–1688.
van den Heuvel MP, Pol HEH. 2010. Exploring the brain network: A review on resting-state fMRI functional connectivity. Eur Neuropsychopharmacol. 20:519–534.
Weigard A, Beltz A, Reddy SN, Wilson SJ. 2019. Characterizing the role of the pre-SMA in the control of speed/accuracy trade-off with directed functional connectivity mapping and multiple solution reduction. Hum Brain Mapp. 40:1829–1843.
Wenzlaff H, Bauer M, Maess B, Heekeren HR. 2011. Neural characterization of the speed - Accuracy tradeoff in a perceptual decision-making task. J Neurosci. 31:1254–1266.
Whitfield-Gabrieli S, Nieto-Castanon A. 2012. Conn: a functional connectivity toolbox for correlated and anticorrelated brain networks. Brain Connect. 2:125–141.
Wiegel P, Kurz A, Leukel C. 2020. Evidence that distinct human primary motor cortex circuits control discrete and rhythmic movements. J Physiol. 598:1235–1251.
Wiener M, Kliot D, Turkeltaub PE, Hamilton RH, Wolk DA, Coslett HB. 2012. Parietal influence on temporal encoding indexed by simultaneous transcranial magnetic stimulation and electroencephalography. J Neurosci. 32:12258–12267.
Witt ST, Laird AR, Meyerand ME. 2008. Functional neuroimaging correlates of finger-tapping task variations: an ALE meta-analysis. Neuroimage. 42:343–356.
Yin HZ, Cheng M, Li D. 2019. The right dorsolateral prefrontal cortex is essential in seconds range timing, but not in milliseconds range timing: An investigation with transcranial direct current stimulation. Brain Cogn. 135.
Yokoi A, Diedrichsen J. 2019. Neural Organization of Hierarchical Motor Sequence Representations in the Human Neocortex. Neuron. 1–13.

Address of Corresponding author

Takashi Hanakawa, PhD., M.D.

Department of Integrated Neuroanatomy and Neuroimaging, Kyoto

University Graduate School of Medicine

E-mail: hanakawa.takashi.2s@kyoto-u.ac.jp

Table 1. Brain activity correlated with tempo-modulated brain activity

Location	Cluster		Peak		MNI coordinates	
	p-value (FWE corrected)	Cluster size	P-value (FWE corrected)	T-value	x, y, z	Anatomy toolbox[a]
Positive association with tapping tempi						
Left M1	<0.001	11916	<0.001	9.82	-33, -22, 64	Left precentral gyrus
Right Cerebellum	<0.001	3169	<0.001	10.64	2, -66, -24	Right cerebellar lobules VI-VII
Negative association with tapping tempi						
Left DLPFC	0.014	478	0.022	6.45	-38, 30, 42	Left middle frontal gyrus
Left ACC	0.020	436	0.073	5.77	-10, 30, 32	Left anterior cingulate gyrus/superior frontal gyrus

[a] Brain regions were determined using the SPM anatomy toolbox (Eickhoff et al. 2005)

Supplementary information 1: Confirmation analysis for co-fluctuation of BOLD signals between both M1s during the tapping tasks

For confirmation of the gPPI analysis, we tested whether the timeseries of the BOLD signals between both M1s were correlated during the tapping tasks. The group-averaged correlation coefficients (*r*) were 0.35 ± 0.18, 0.35 ± 0.18, 0.34 ± 0.13, 0.44 ± 0.21 and 0.52 ± 0.18, (mean ± SD) for 0.25, 1, 2, 3 and 4 Hz, respectively. A one-way repeated measures analysis of variance (ANOVA) for the comparison of correlation coefficient values found a significant main factor of TAPPING TEMPO (0.25-4 Hz) ($F_{2.33, 22}$ = 8.91, p = 0.0002). Post-hoc explanations showed that the correlation coefficients were significantly higher towards 4Hz (0.25 Hz vs 4 Hz, t = 3.73, p = 0.006; 1 Hz vs 4 Hz, t = 3.73, p = 0.006; 2 Hz vs 4 Hz, t = 4.57, p = 0.001, after Bonferroni correction). The result of this complementary analysis indicated that even though the ipsilateral M1 activity did not reach significance, the change of activity was correlated between bilateral M1s during rhythmic movement.

Supplementary Table 1: Number of finger taps for each condition and correlations between the number of finger taps and the CV value

Condition	Number of finger taps for each block (20s) (mean ± SE)	correlation between the number of finger taps and the CV value			
		correlation coefficient	95% CI		significant correlation
1Hz	19.3 ± 0.13	-0.01	-0.38	0.42	n.s.
2Hz	38.9 ± 0.25	-0.35	-0.64	0.13	n.s.
3Hz	58.3 ± 0.19	-0.27	-0.64	0.01	n.s.
4Hz	79.7 ± 0.76	-0.04	-0.50	0.43	n.s.

95% CI: 95% confidence interval, n.s.: not significant correlation, SE: standard error

Supplementary Figure 1

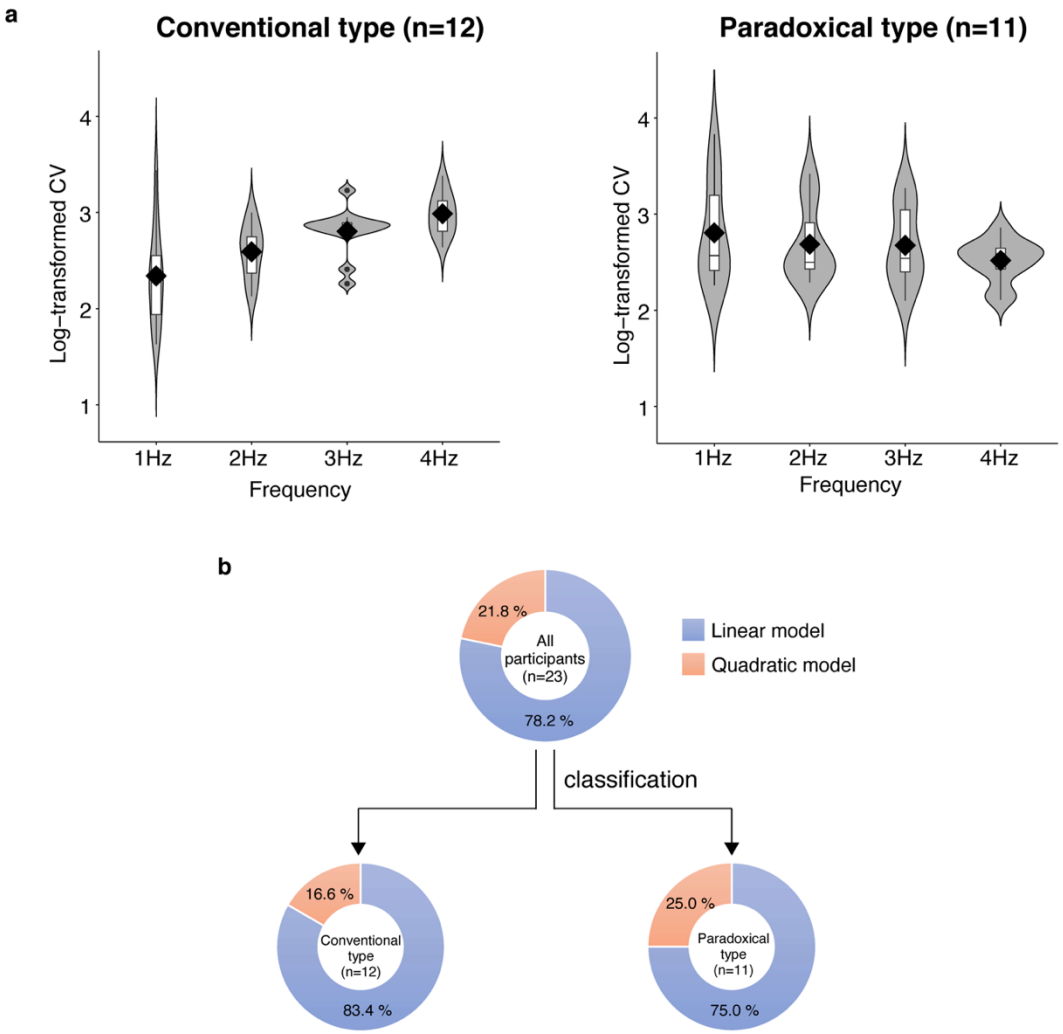

Changes in the CV values classified into two groups: a. Changes in the CV values in response to tapping tempi were classified into the conventional and paradoxical groups according to the *slop* of TRF. Violin plots showing log-transformed CVs for ITIs in each tempo. Participants who were assigned to the conventional type showed that precision motor rhythmicity at lower tempi was less precision at higher tempi. Whereas, participants from the paradoxical type showed that imprecise motor rhythmicity (a high CV) at lower tempi improved rhythmicity at faster tempi. A higher value indicates more disruption of motor rhythmicity during finger tapping. The boxes indicate the interquartile ranges. The black diamonds and the error bars indicate the mean and SD, respectively. The violin-shaped areas indicate data density. **b.** A breakdown of the behavioral models. The linear model was superior to the quadratic model for about 80% of participants, regardless of group.

Supplementary Figure 2

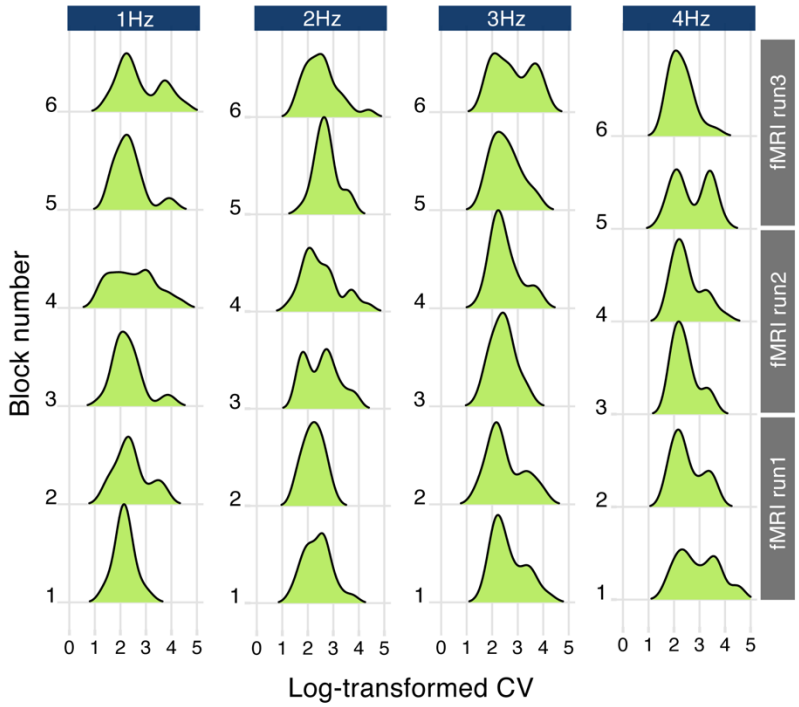

Changes in CV for each tapping tempo throughout the data collection: The density plots depict the distribution of CV values obtained from the 23 participants. To clarify any motor learning effects, we performed a two-way repeated measures ANOVA with BLOCK (1-6 blocks) and TAPPING TEMPO (1-4Hz) as within-subjects factors. This analysis yielded a significant main effect of BLOCK ($F_{3.7, 82.9} = 3.73$, $p=0.04$) and no significant main effect of TAPPING TEMPO ($F_{2.2, 50.1} = 2.83$, $p=0.06$), adjusted by Greenhouse-Geisser correction as the assumption of sphericity was violated. However, post-hoc explorations of the main effect of BLOCK did not find any significant blocks. CV at block #5 tended to be smaller than that at block #6. CVs at blocks #1 and #2 tended to be greater than that at block #5. CV at block #1 tended to be greater than that at block #3. These statistical results indicate that the CV values are unlikely to be influenced by the motor learning effect.

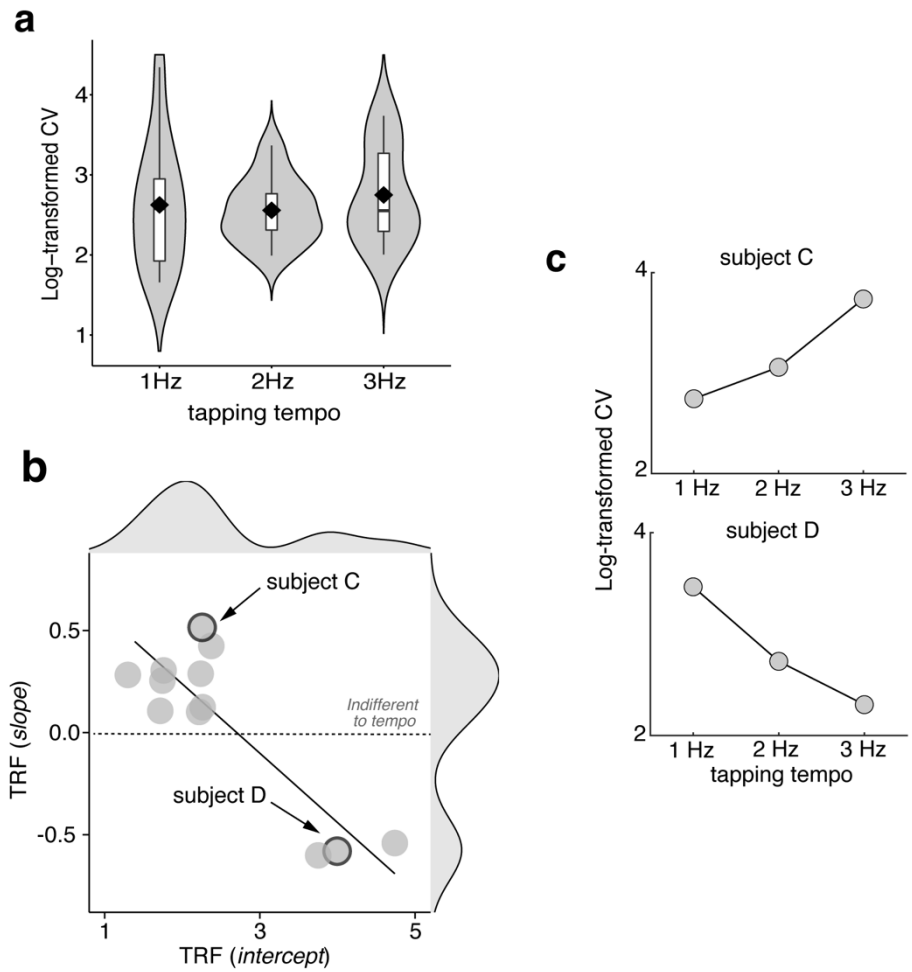

Confirmation of behavior in a different cohort: a, Violin plots showing log-transformed CVs for ITIs in each tempo that were made from other independent cohort (n=12). A higher value indicates more disruption of motor rhythmicity during finger tapping. The boxes indicate the interquartile ranges. The black diamonds and the error bars indicate the mean and SD, respectively. The violin-shaped areas indicate data density. **b,** A scatterplot showing the relationship between the *slope* and *intercept* of the TRF. Marginal density plots of x-axes (top panel) and y-axes (right panel) indicate the distribution of the *intercept* and *slope* values, respectively. One dot represents data from one participant. For the y-axis, positive values indicate that rhythmicity was disrupted by the increase in tapping tempo, while negative values indicate that rhythmicity was improved by the increase in tapping tempo. For the x-axis, high values indicate imprecise rhythmicity at a slow tempo (i.e., discrete movement). **c,** Typical examples of changes in CVs across the given tapping tempi from representative participants are shown (subject C and D).

Supplementary Figure 4

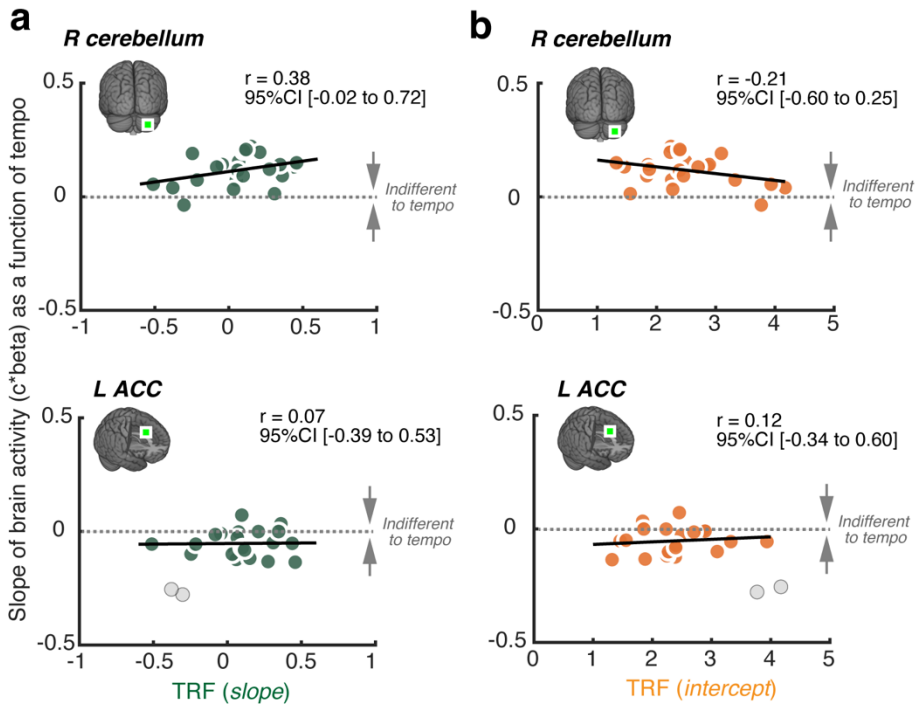

The relationships between tempo-modulated brain activity and TRF parameters (no-significant results): The relationships between tempo-modulated brain activity and the TRF, including the *slope* **(a)** and the *intercept* **(b),** are plotted on a scatterplot concerning each brain region. No significant correlations were found in the left cerebellar lobules VI–VII or left ACC, irrespective of the *slope* or *intercept* of the TRF. Pearson's correlation was applied using a bootstrapped method. Correlations were considered significant if the 95% CI did not include zero. One dot represents data from one participant. Outliers are displayed as a gray dot.

Supplementary Figure 5

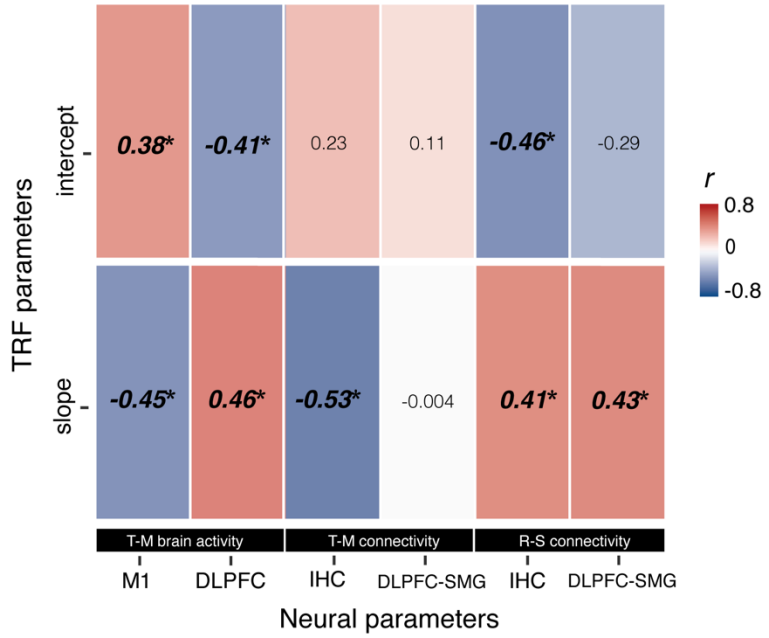

Summary of the series of correlation analyses: Each correlation coefficient (r) shown in Figures 3-5 is summarized in a heatmap, where deeper red and blue indicate positive and negative correlations, respectively. T-M: tempo-modulated; R-S: resting-state. Significant correlations are indicated in bold and italics with an asterisk.